Tu A18

Spatiotemporal Adaptive Multiscale Multiphysics Simulations of Two-phase Flow

P. Tomin* (University of Lausanne) & I. Lunati (University of Lausanne)

SUMMARY

We present a spatiotemporal adaptive multiscale algorithm, which is based on the Multiscale Finite Volume method. The algorithm offers a very efficient framework to deal with multiphysics problems and to couple regions with different spatial resolution. We employ the method to simulate two-phase flow through porous media. At the fine scale, we consider a pore-scale description of the flow based on the Volume Of Fluid method. In order to construct a global problem that describes the coarse-scale behavior, the equations are averaged numerically with respect to auxiliary control volumes, and a Darcy-like coarse-scale model is obtained. The space adaptivity is based on the idea that a fine-scale description is only required in the front region, whereas the resolution can be coarsened elsewhere. Temporal adaptivity relies on the fact that the fine-scale and the coarse-scale problems can be solved with different temporal resolution (longer time steps can be used at the coarse scale). By simulating drainage under unstable flow conditions, we show that the method is able to capture the coarse-scale behavior outside the front region and to reproduce complex fluid patterns in the front region.

Introduction

Multiphase flow through porous media is characterized by a variety of scales. Multiscale methods (e.g. the Multiscale Finite Volume (MsFV) method (Jenny et al., 2003)) have been developed to efficiently deal with situation in which these scales are coupled and traditional upscaling techniques are not effective. Recently, the MsFV method has been extended (Tomin and Lunati, 2013) for multiphysics (hybrid) applications, and it has been used to dynamically couple a Darcy-scale model to a pore-scale model that aims at describing the flow with sub-pore spatial resolution.

Although, the two-phase flow patterns may be very complex (Ferrari and Lunati, 2013), particularly for unstable flow regimes, it is always possible to identify regions where the fluid distribution does not significantly change, while active redistribution takes place in a front region, which characterized by a typical length l_f. If $l_f \ll L_\Omega$ (where L_Ω is the domain size) a detailed (pore-scale) description of the flow is not required in most of the domain and methods that employ an adaptive spatial resolution (Fig. 1) become very attractive as they allow a substantial reduction of the computational costs (Lee et al., 2009; Künze and Lunati, 2012; Künze et al., 2014).

The main idea of spatially adaptivity is to coarsen the description far from the front region, while keeping a finer resolution where active fluid redistribution takes place. The use of different spatial scales implies the use of different temporal scales, and we have recently proposed a spatiotemporal adaptive MsFV method (Tomin and Lunati, 2014), which relies on a local-global splitting of the original system of equations. In this framework, we define a set of local problems that are coupled through their boundary conditions, which are obtained by the solution of global problem and the use of numerically computed interpolators. The local-global splitting allows us to retain the original degree of coupling in the local subdomain and makes it easier to locally employ different descriptions as required by the actual flow conditions.

Governing equations

We consider the flow of two incompressible phases trough a rigid solid matrix. At the pore-scale the flow is described by the whole-domain formulation (see, e.g., Scardovelli and Zalesky (1999); Lafaurie et al. (1994)), which treats the two-phase system as a single fluid with properties that vary in space depending on the phase that is present. The phase distribution is described by a fluid function, α, which represents the volumetric fraction of one of the two phases (e.g., phase 1). The density and the viscosity are

$$\rho = \alpha\rho_1 + (1-\alpha)\rho_2, \qquad \mu = \alpha\mu_1 + (1-\alpha)\mu_2, \tag{1}$$

respectively, where ρ_i is the constant density and μ_i is the constant viscosity of the i-phase.

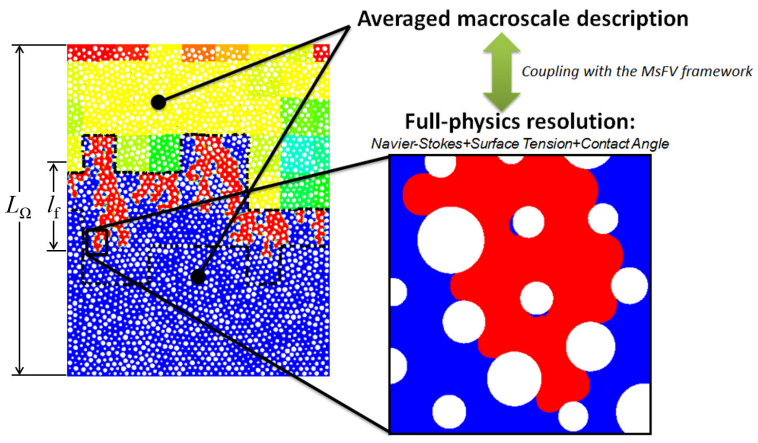

Figure 1 *A pictorial representation of adaptive resolution for multiphysics problems.*

The flow is described by the following conservation equations:

1. The total mass conservation equation,
$$\nabla \cdot \boldsymbol{u} = 0, \tag{2}$$
which is expressed in form of a volume conservation equation and reduces to a divergence-free condition on the velocity.

2. The momentum balance equation
$$\frac{\partial \rho \boldsymbol{u}}{\partial t} = -\nabla p + \nabla \cdot \mu \left(\nabla \boldsymbol{u} + \nabla \boldsymbol{u}^T \right) + \gamma \kappa \nabla \alpha, \tag{3}$$
where the last term on the right-hand side accounts for the surface force acting at the fluid-fluid interface (γ is the surface tension, and $\kappa = -\nabla \cdot \boldsymbol{n}_\alpha = \nabla \cdot (\nabla \alpha / |\nabla \alpha|)$ is the total curvature of the interface) and where we have neglected the non-linear term since the Reynolds number is small.

3. The mass conservation equation for phase 1,
$$\frac{\partial \alpha}{\partial t} + \nabla \cdot (\alpha \boldsymbol{u}) = 0, \tag{4}$$
which has the form of a simple advection equation for the fluid function α.

To be solved for pressure, p, velocity, $\boldsymbol{u}$, and fluid funtion, α, Eqs. 2–4 have to be supplemented with appropriate boundary conditions. On the solid boundary, $\partial \Omega^s$, the no-slip condition is imposed for the velocity,
$$\boldsymbol{u}|_{\partial \Omega^s} = 0, \tag{5}$$
whereas the normal to the fluid-fluid interface, $\boldsymbol{n}_\alpha$, is fixed and determined by the contact angle, θ_{eq}, to describe the effects of wetting. The pore-scale simulations presented in the following are performed with a modified implementation of the open-source software package OpenFOAM (2012).

Local-global splitting

The main idea is to decompose the original problem into a set of local problems that are solved on subdomains, $\bar{\Omega}_i$, defined by the cells of an auxiliary coarse grids (Fig. 2), and coupled through the boundary conditions. The set of localized problems can be written in matrix form as
$$A_\ell x = r + (A_\ell - A) x_{\text{bc}}, \tag{6}$$

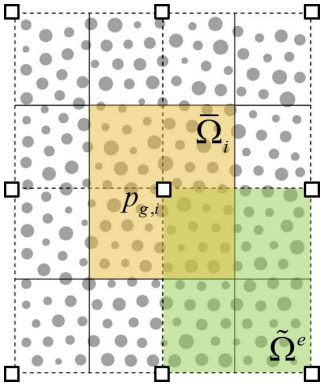

Figure 2 *Coarse grid (solid) and dual grid (dashed). (The underlying fine grid that resolve the pore space is not shown here.)*

where $x = \begin{bmatrix} p & u & \alpha \end{bmatrix}^T$ is the vector of the unknowns; A is the matrix representing the discretization of the orginal problem; r is the right-hand-side vector; A_ℓ is the operator which is constructed from A by removing the connections across coarse cells and contains all the decoupled local problems (Lunati and Lee, 2009); and $x_{\rm bc}$ is the vector from which the boundary conditions of the local problems are computed.

The vector $x_{\rm bc}$ is obtained by solving a global problem, which is constructed by projecting the fine-scale problem onto the coarse grid, i.e.,

$$\chi A x_{\rm bc} = \chi r, \tag{7}$$

where the restriction operator χ sums up all fine-scale values corresponding to the same coarse cell. In following we assume that only coarse pressure values, $p_{\rm g}$, are relevant degrees of freedom at the global scale (Tomin and Lunati, 2013), and we write

$$x_{\rm bc} = \begin{bmatrix} p_{\rm bc} \\ u_{\rm bc} \\ \alpha_{\rm bc} \end{bmatrix} = \begin{bmatrix} \mathscr{B}_p \\ \mathscr{B}_u \\ 0 \end{bmatrix} p_{\rm g} + \mathscr{C} r. \tag{8}$$

where $\mathscr{C}$ is the correction function operator (Lunati and Jenny, 2008; Lunati and Lee, 2009); and the columns of the basis-function operators, $\mathscr{B}_p$ and $\mathscr{B}_u$, contain the interpolators of the pressure and the velocity, respectively, and are computed by simultaneous solution of Eqn. 2–3 for each degree of freedom. The construction of interpolators is briefly discussed in the next section; we refer to (Tomin and Lunati, 2013) for further details.

Taking into account the hyperbolic nature of Eq. 4, no interpolator is introduced for fluid function ($\mathscr{B}_\alpha = 0$), and the boundary conditions for localized transport problems, $\alpha_{\rm bc}$, are obtained from the solution at previous time. Formally this is described by applying the correction-function operator to the right-hand side, r, which contains $\alpha_{\rm bc}$ at the previous time.

Substituting Eq. 8 into Eq. 7, we have the global-pressure problem

$$(\chi_p A \mathscr{B}) p_{\rm g} = \chi_p (I - A\mathscr{C}) r, \tag{9}$$

where we have added the subscript to χ_p to indicate that only the global equation for pressure is constructed. This equation can be written in a simple Darcy-like form

$$\sum_{j \neq i} T_{ij} \left(p_{g,i} - p_{g,j} \right) = F_i, \quad i = 1..N_c, \tag{10}$$

where the coarse transmissibilities, T_{ij}, can be seen as an extension of Darcy-scale total mobilities as they depend on the fine-scale distribution of the fluids and also include relaxation effects since the basis-functions are obtained by solving time-dependent equations.

Once the global problem is solved, the boundary conditions for the full system of equations are constructed from Eq. 8 and used to locally solve the full system of pore-scale equations 2–4 on coarse cells (Fig. 3). The solvability is ensured by the consistency between the integral pore-scale and coarse-scale fluxes, and by the fact that momentum always can be dissipated on solids.

Definition of interpolators

The interpolators are calculated on the dual coarse cells, $\tilde{\Omega}_e$, (Fig. 2) and provide a numerical closure to the coarse problem (generalizing Darcy's law). In each dual cell, $\tilde{\Omega}^e$, we use the decompositions

$$p_{\rm bc} = \sum_{i=1}^{N_c^e} p_{g,i} \phi_i^e + \phi_0^e, \qquad \text{and} \qquad \boldsymbol{u}_{\rm bc} = \sum_{i=1}^{N_c^e} p_{g,i} \boldsymbol{\psi}_i^e + \boldsymbol{\psi}_0^e. \tag{11}$$

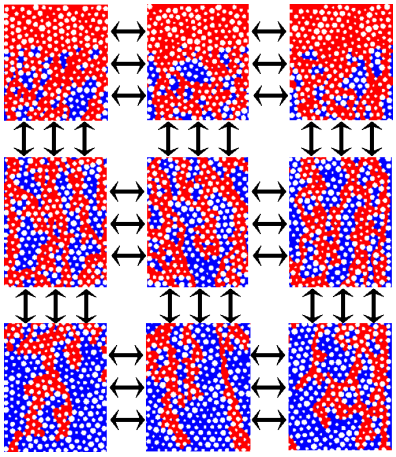

Figure 3 *Local sub-problems are coupled by boundary fluxes.*

where N_c^e is the number of dual-cell nodes ($N_c^e = 2^d$ in case of a Cartesian grid, where d is the number of dimensions); ϕ_i^e and $\boldsymbol{\psi}_i^e$ are the basis functions, and ϕ_0^e and $\boldsymbol{\psi}_0^e$ the correction functions for pressure and velocity, respectively. The constrains

$$\sum_{i=1}^{N_c^e} \phi_i^e = 1, \qquad \text{and} \qquad \sum_{i=1}^{N_c^e} \boldsymbol{\psi}_i^e = \mathbf{0}, \tag{12}$$

allow us to solve only N_c^e independent problems for the interpolators ($N_c^e - 1$ basis functions and one correction function).

For a given distribution of the fluid function, α, and with initial and boundary conditions summarized in Tab. 1, pressure and velocity basis functions are the local solutions in each dual cell, $\tilde{\Omega}^e$, of the system

$$\begin{cases} \nabla \cdot \boldsymbol{\psi}_i^e = 0, \\ \rho(\alpha) \dfrac{\boldsymbol{\psi}_i^e}{\Delta t} = -\nabla \phi_i^e + \nabla \cdot \left[\mu(\alpha) \left(\nabla \boldsymbol{\psi}_i^e + \nabla \boldsymbol{\psi}_i^{eT} \right) \right], \end{cases} \tag{13}$$

whereas the correction functions are obtained by solving

$$\begin{cases} \nabla \cdot \boldsymbol{\psi}_0^e = 0, \\ \rho(\alpha) \dfrac{\boldsymbol{\psi}_0^e - \check{\boldsymbol{v}}}{\Delta t} = -\nabla \phi_0^e + \nabla \cdot \left[\mu(\alpha) \left(\nabla \boldsymbol{\psi}_0^e + \nabla \boldsymbol{\psi}_0^{eT} \right) \right] + \gamma \kappa \nabla \alpha. \end{cases} \tag{14}$$

where $\check{\boldsymbol{v}}$ is the velocity at previous time step. The treatment of the time derivative used above is similar to the one proposed to simulate compressible Darcy flow (Hajibeygi and Jenny, 2009). An example of pressure and velocity basis functions is shown in Fig. 4.

	$(\phi, \boldsymbol{\psi})_{1-N_c^e}$	$(\phi, \boldsymbol{\psi})_0$
Initial conditions	$\boldsymbol{\psi}_i = \mathbf{0}$	$\boldsymbol{\psi}_0 = \check{\boldsymbol{v}}$
Boundary conditions	$\phi_i = 1$ for node i, $\phi_i = 0$ for all other nodes of $\tilde{\Omega}^e$, linear ϕ_i bet-ween the nodes	$\phi_0 = 0$
	zero normal gradient for $\boldsymbol{\psi}_i$	
Surface tension	$\gamma = 0$	$\gamma \neq 0$

Table 1 *The summary of initial and boundary conditions for interpolators.*

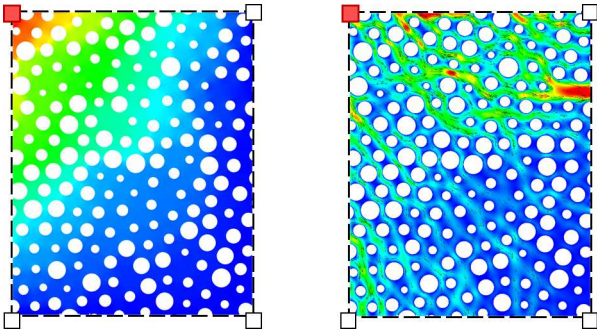

Figure 4 *Pressure (left) and velocity (right) basis functions.*

Spatial adaptivity

In the MsFV framework, interpolators are selectively updated based on total-mobility variations in fine cells (Jenny et al., 2004, 2006; Lunati and Jenny, 2006; Lee et al., 2009). This fine-scale criterion is efficient only for moderate ratios between fine-cell and coarse-cell sizes. In case of large ratios, which is usually the case in multiphysics applications (Tomin and Lunati, 2013), the large-scale effects of fine-scale changes might be negligible and criteria based on coarse-scale quantities must be devised. Therefore, we update the interpolators based on coarse-scale variations of the average saturation.

In addition to the selective update of the interpolators, we employ an adaptive spatial resolution: outside the front region, local problems are not solved and only a coarse-scale solution is computed. To identify the front region and decide where a fine-scale resolution is required, we monitor time evolution of the fluid saturation in the cell $\bar{\Omega}_i$. Therefore, we coarsen the resolution if

$$\left|\frac{\Delta S_i}{\Delta t}\right| < \varepsilon_t. \tag{15}$$

where $S_i = \int_{\bar{\Omega}_i} \alpha \, dV$ is the saturation of the cell i, and ΔS_i is its variation over the time step Δt. (The criterion in Eq. 15 is similar to the one employed in (Lee et al., 2009) for adaptive transport, but we consider the time derivative and not the absolute change of saturation.)

Temporal adaptivity

As a consequence of the different spatial scales, the typical time scale of fine and coarse problems are different, which suggests to use different time step for the local problems and for the global problem. Indeed, local problems require smaller time steps, Δt_l, to correctly describe the dynamics of two phases in the pore space. However, it is in general not necessary to frequently update the global solution, p_g, which can be computed with larger time step, ΔT_g. This means that the first term in right-hand side of Eq. 8 is updated only every $G = \Delta T_g / \Delta t_l \geq 1$ local time steps. To decide whether boundary conditions have to be updated, we employ a criterion based on pressure-gradient changes, which provide an indirect estimate of coarse-scale mobility changes (Tomin and Lunati, 2014). Therefore, we construct and solve the coarse problem to update the boundary conditions if

$$\max_i \frac{\left|\Delta \langle \nabla p \rangle_{\bar{\Omega}_i}\right|}{\left|\langle \nabla p \rangle_{\bar{\Omega}_i}\right|} = \max_i \frac{\left|\Delta \oint_{\partial \bar{\Omega}_i} p \boldsymbol{n} dS\right|}{\left|\oint_{\partial \bar{\Omega}_i} p \boldsymbol{n} dS\right|} > \varepsilon_{\nabla p}. \tag{16}$$

This criterion requires that the relative change in the net pressure force applied at the cell boundary, $\partial \bar{\Omega}_i$, does not exceed a certain threshold value, $\varepsilon_{\nabla p}$. Since total fluxes across the boundary are fixed, changes in net applied force imply changes in the total mobility of the coarse cell $\bar{\Omega}_i$. The temporal adaptivity is investigated in great details in (Tomin and Lunati, 2014). Notice that updating the boundary conditions

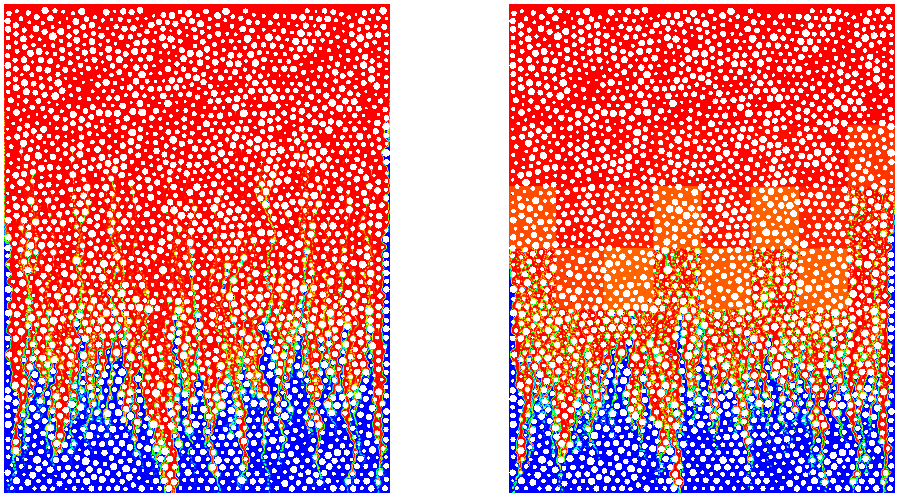

Figure 5 *Tracer transport problem: reference solution (left) and adaptive multiscale solution (right).*

for the fluid function does not require solving the global problem because they are simply extracted from the fluid-function distribution at the previous time; therefore, they are updated at every fine-scale time step.

Numerical simulations

Tracer transport

First, we test the adaptive resolution algorithm for an ideal tracer transport problem. The tracer is injected at the top boundary and then transported in accordance to the fixed velocity field. The pore geometry is idealized by circular obstacles and its properties are summarized in Tab. 2. To avoid large numerical dispersion, an artificial compression term is added in Eq. 4 (Rusche, 2002). The coarse grid in the multiscale solution has 8×8 cells. The value of the adaptivity threshold is $\varepsilon_t = 10^{-2}$. The fine-scale reference solution and solution of the adaptive multiscale approach are shown in Fig. 5. They are in very good agreement with each other and they qualitatively agree with experiments for similar geometries (Birovljev et al., 1994; de Anna et al., 2014).

Two-phase flow

Next, we simulate drainage in the same pore geometry. Since the stable displacement regime is trivial, we focus on unstable regime, in which the viscosity ratio is slightly unfavorable, i.e., $M = \mu_{\mathrm{nw}}/\mu_{\mathrm{w}} = 0.2$. The non-wetting fluid is injected at the top boundary at constant inlet velocity $v_{\mathrm{in}} = 10^{-2}$ m/s, whereas the pressure is fixed at the outlet, $p_{\mathrm{out}} = 0$. The pore-scale Reynolds number is $Re \sim 0.01$, and the capillary number is $Ca \sim 0.1$.

We present the results for two values of the spatial adaptivity thresholds: $\varepsilon_t = 10^{-2}$ and $\varepsilon_t = 10^{-3}$. A pore to pore comparison is not very informative for unstable regimes because small differences grow with time; therefore, we evaluate the results in terms of vertical saturation profiles, which are obtained by averaging the fluid distribution horizontally (Fig. 6). The reference solution is obtained by direct fine-scale simulation. The coarse grid in the multiscale solution has 9×10 cells. Although the lowest

Table 2 *Pore geometry properties.*

Domain size	Mean obstacle size	Mean pore throat size	Number of obstacles	Number of cells	Permeability	Porosity
45 mm $\times$ 56.8 mm	0.6 mm	0.4 mm	2 507	711 720	10^{-8} m^2	70%

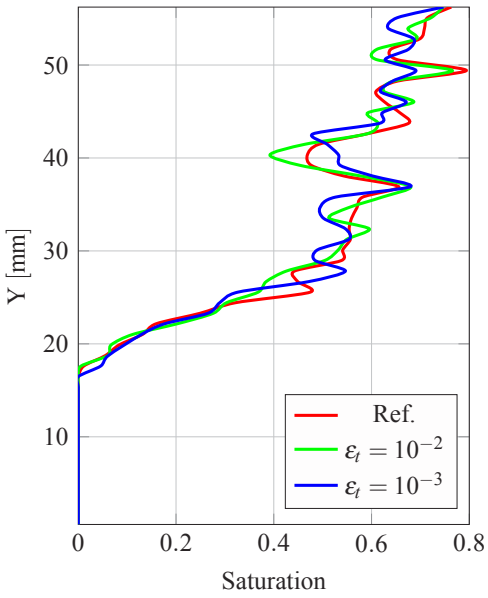

Figure 6 *Horizontally averaged saturation profile at $t = 1.5$ s.*

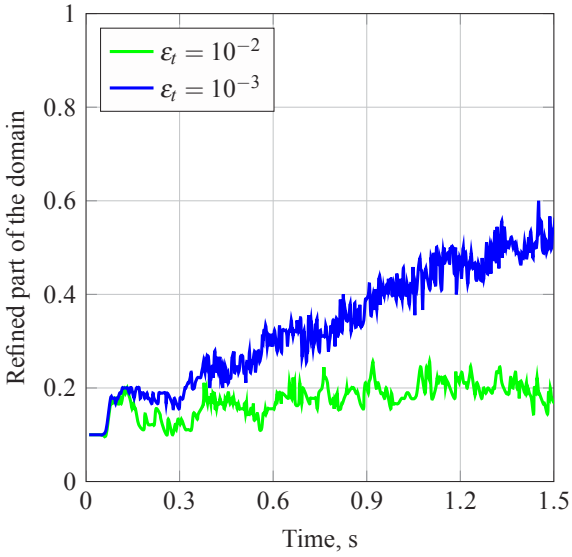

Figure 7 *Fraction of the domain that has to be refined as a function of time for two adaptivity thresholds.*

adaptivity threshold values yield slightly more accurate results, the main flow characteristics (e.g., the penetration depth) are well captured by using both thresholds. At the same time, $\varepsilon_t = 10^{-2}$ leads to the refinement of only about 18% of the domain, and this value remains almost constant with time (green line in Fig. 7); in contrast, $\varepsilon_t = 10^{-3}$ requires refining in average 35% of the domain and the refined fraction clearly increases with time (blue line in Fig. 7). In both cases, we used $\delta_{\nabla p} = 0.2$ for temporal adaptivity, which improves the efficiency and leads to the average time-step ratio $G = 20.2$ in case of more refined solution, $\varepsilon_t = 10^{-3}$, and $G = 41.8$ when $\varepsilon_t = 10^{-2}$ is used.

Finally, the adaptive multiscale solution at the end of the simulation (obtained with $\varepsilon_t = 10^{-2}$ and $\delta_{\nabla p} = 0.2$) is compared with the fine-scale reference in Fig. 8, which shows the fluid-function distributions. The two solutions are in good agreement and the main flow characteristics observed in the reference solution are satisfactorily reproduced by the adaptive multiscale algorithm.

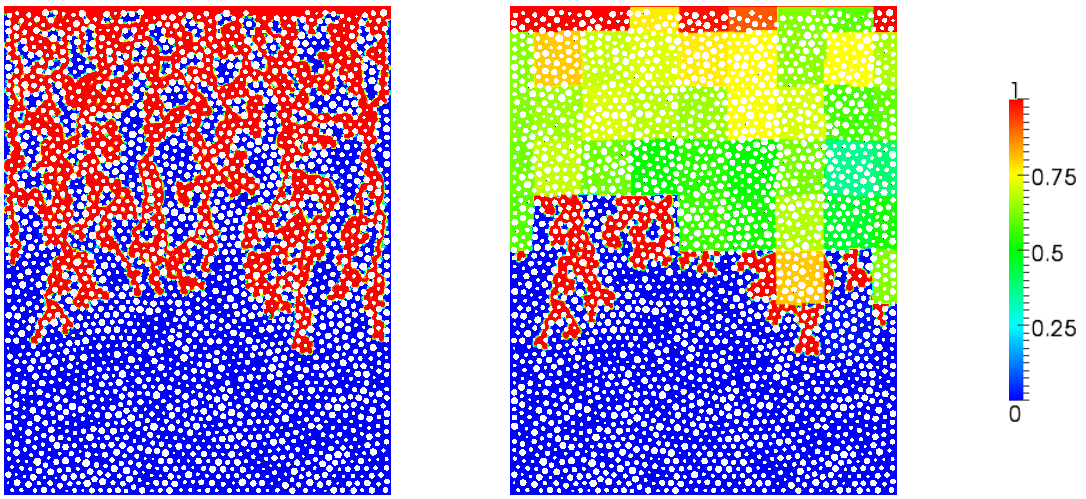

Figure 8 *Two-phase flow: reference solution (left) and adaptive multiscale solution (right).*

Conclusions

We have presented an adaptive multiphysics algorithm, which is based on the MsFV method. As we employ a local-global splitting of the original system of equations, we are able to use a scheme that is adaptive in space and time and can effectively describe unstable flow regimes. Space adaptivity mostly rely on the coarsening of the solution outside a front region. For the case considering here, this allows us to use a pore-scale description of the flow in the front region, while a Darcy-like description is used elsewhere. Temporal adaptivity is motivated by the simple observation that the characteristic time of the global (coarse-scale) problem is longer than characteristic time of the local (fine-scale) problems. This allows us to update the boundary condition less frequently, and improves the efficiency of the algorithm by reducing the number of times that the global pressure solution has to be calculated.

The numerical solutions obtained with the adaptive method are in good agreement with the reference solutions obtained with a fine-scale solver. The proposed method is very efficient when the front region is relatively compact and much smaller than the entire domain.

Acknowledgements

The work is supported by the Swiss National Science Foundation grant PP00P2_144922.

References

Birovljev, A., Måløy, K. J., Feder, J. and Jøssand, T. [1994] Scaling structure of tracer dispersion fronts in porous media. Physical Review E 49(6), 5431–5437.

de Anna, P., Dentz, M., Tartakovsky, A. and Le Borgne, T. [2014] Filamentary structure of mixing fronts controls reaction kinetics in porous media flows. Geophysical Research Letters, doi: 10.1002/2014GL060068 .

Ferrari, A. and Lunati, I. [2013] Direct numerical simulations of interface dynamics to link capillary pressure and total surface energy. Advances in Water Resources 57, 19–31.

Hajibeygi, H. and Jenny, P. [2009] Multiscale finite-volume method for parabolic problems arising from compressible multiphase flow in porous media. Journal of Computational Physics 228(14), 5129–5147.

Jenny, P., Lee, S. H. and Tchelepi, H. A. [2003] Multi-scale finite-volume method for elliptic problems in subsurface flow simulation. Journal of Computational Physics 187(1), 47–67.

Jenny, P., Lee, S. H. and Tchelepi, H. A. [2004] Adaptive multiscale finite-volume method for multi-phase flow and transport in porous media. Multiscale Modeling and Simulation 3(1), 50–64.

Jenny, P., Lee, S. H. and Tchelepi, H. A. [2006] Adaptive fully implicit multi-scale finite-volume method for multi-phase flow and transport in heterogeneous porous media. Journal of Computational Physics 217(2), 627–641.

Künze, R. and Lunati, I. [2012] An adaptive multiscale method for density-driven instabilities. Journal of Computational Physics 231, 5557–5570.

Künze, R., Tomin, P. and Lunati, I. [2014] Local modeling of instability onset for global finger evolution. Advances in Water Resources 70, 148–159.

Lafaurie, B., Nardone, C., Scardovelli, R., Zaleski, S. and Zanetti, G. [1994] Modelling merging and fragmentation in multiphase flows with SURFER. Journal of Computational Physics 113, 134–147.

Lee, S. H., Zhou, H. and Tchelepi, H. A. [2009] Adaptive multiscale finite-volume method for nonlinear multiphase transport in heterogenous formations. Journal of Computational Physics 228(24), 9036–9058.

Lunati, I. and Jenny, P. [2006] Multi-scale finite-volume method for compressible flow in porous media. Journal of Computational Physics 216(2), 616–636.

Lunati, I. and Jenny, P. [2008] Multiscale finite-volume method for density-driven flow in porous media. Computational Geosciences 12(3), 337–350.

Lunati, I. and Lee, S. [2009] An operator formulation of the multiscale finite-volume method with correction function. Multiscale Modeling and Simulation 8(1), 96–109.

OpenFOAM [2012] The Open Source CFD Toolbox: User Guide. OpenFOAM Foundation, version 2.1.1.

Rusche, H. [2002] Computational fluid dynamics of dispersed two-phase flows at high phase fractions. Ph.D. thesis, Imperial College London.

Scardovelli, R. and Zalesky, S. [1999] Direct numerical simulation of free-surface and interfacial flow. Annual Review of Fluid Mechanics 31, 567–603.

Tomin, P. and Lunati, I. [2013] Hybrid multiscale finite volume method for two-phase flow in porous media. Journal of Computational Physics 250, 293–307.

Tomin, P. and Lunati, I. [2014] Local-global splitting for spatiotemporal-adaptive multiscale methods. Journal of Computational Physics .